Available online at www.sciencedirect.com
SCIENCE DIRECT®
PERGAMON
International Journal of Rock Mechanics & Mining Sciences 41 (2004) 69–87
International Journal of Rock Mechanics and Mining Sciences
www.elsevier.com/locate/ijrmms

Numerical analysis of initiation and progressive failure in natural rock slopes—the 1991 Randa rockslide

E. Eberhardt[a,*], D. Stead[b], J.S. Coggan[c]

[a] Engineering Geology, Swiss Federal Institute of Technology (ETH Zurich), Zurich, CH 8093, Switzerland
[b] Earth Sciences, Simon Fraser University, Vancouver, BC, Canada
[c] Camborne School of Mines, University of Exeter, Cornwall, UK

Accepted 12 May 2003

Abstract

The 1991 Randa rockslide in the Swiss Alps involved several complex mechanisms relating to geological, mechanical and hydrological processes for which no clear trigger can be asserted. This paper investigates the concept of progressive failure and the numerical modelling of rock mass strength degradation in natural rock slopes using the Randa rockslide as a working example. Results from continuum (i.e. finite-element) modelling are presented to illustrate a hypothesis, suggesting that initiation of a progressive rock mass degradation process, ultimately leading to failure, began following deglaciation of the valley below. Discontinuum (distinct-element) modelling is then applied to investigate the underlying mechanisms contributing to the episodic nature of the rockslide. Finally, the use of a hybrid method that combines both continuum and discontinuum techniques to model fracture propagation are discussed in the context of modelling progressive slide surface development linking initiation and degradation to eventual catastrophic failure.
© 2003 Elsevier Ltd. All rights reserved.

1. Introduction

In rock slope stability analyses, the failure surface is often assumed to be structurally controlled and predefined as a continuous plane or series of interconnected planes. The justification for this is part due to post-failure observations where fully persistent discontinuities are fitted to the failure surface to explain its origin in a geological context, and partly due to the constraints of the analysis technique employed (many of which require the input of fully persistent discontinuities; e.g. limit equilibrium wedge or planar analysis, distinct-element method, etc.). Such assumptions are often only valid in cases where the volume of the failed block is relatively small (e.g. thousands of m^3) or where major persistent faults and/or bedding planes are present.

In massive natural rock slopes and deep, engineered slopes (e.g. open pit mines), it is highly unlikely that such a network of fully persistent natural discontinuities exist a priori to form a complete 3-D surface enabling kinematic release. Instead, Terzaghi [1], Robertson [2], Einstein et al. [3] and others suggest that the persistence of key discontinuity sets is in reality more limited and that a complex interaction between existing natural discontinuities and brittle fracture propagation through intact rock bridges is required to bring the slope to failure.

Eberhardt et al. [4] argue that such processes must be considered to explain the temporal nature of massive natural rock slope failures. For example, in small engineered slopes, the rock mass may be continuously disturbed by excavation and fully persistent discontinuities may be exposed/daylighted enabling kinematic feasibility. However, natural rock slopes do not experience such rapid changes to their kinematic state and frequently have stood in a relatively stable condition over periods of thousands of years (e.g. since deglaciation). This is not to say that in a natural rock slope a system of natural discontinuities may not be interconnected forming a significant portion of what will eventually be the failure surface, but that a component of strength degradation with time must also occur within the rock mass driving the slope towards a disequilibrium condition and unstable state.

*Corresponding author. Tel.: +41-1-633-2594; fax: +41-1-633-1108.
E-mail address: erik@erdw.ethz.ch (E. Eberhardt).

1365-1609/03/$ - see front matter © 2003 Elsevier Ltd. All rights reserved.
doi:10.1016/S1365-1609(03)00076-5

As such, massive rock slope instability inherently requires the progressive degradation and destruction of cohesive elements, for example intact rock bridges, to bring the slope to catastrophic failure. This paper explores the concept of progressive failure in natural rock slopes and examines the inclusion of strength degradation in the modelling of process initiation and massive failure, focussing on the example of the 1991 Randa rockslide in the southern Swiss Alps.

2. Progressive failure in natural rock slopes

2.1. Background and conceptual considerations

The concept of progressive slope failure was originally introduced to explain discrepancies between average shear stresses back-calculated along failure surfaces in overconsolidated clay slopes and shear strengths of the same clay material in laboratory testing. Bjerrum [5] summarized in his Terzaghi lecture that failure in such cases must be preceded by the development of a continuous sliding surface through the progressive propagation of a shear surface along which shear strength is reduced from peak to residual values (Fig. 1). This model implies a gradual development of the eventual failure plane.

In rock slopes, Terzaghi [1] emphasized that most rock masses contain discontinuous joints varying in persistence, such that both their stress-conditioned shearing resistance (i.e. the frictional strength component) and the cohesion of intact rock bridges between discontinuous joints (referred to as *effective cohesion* along the shear surface) combine to resist shear failure. Mathematically, effective cohesion can be written as

$$c_i = c\frac{A_g}{A}, \tag{1}$$

where c is the intact rock cohesion, A_g represents the total area of the gaps formed between discontinuities (i.e. area of the intact rock bridges) along the shear surface and A is the total area of the shear surface. Progressive failure in massive rock slopes would therefore entail the failure of individual rock bridges as their shear strength was exceeded. Stresses ahead of the shear plane would increase and subsequent intact rock bridges fail in a consecutive manner until the surface of failure extended to the point where kinematic release became possible.

Rock slope analyses relating to these principles have been forwarded in several studies. Most involve the derivation of limit equilibrium solutions based on the Coulomb shear strength criterion, adopting an apparent cohesion dependent on the continuity of jointing (e.g. [1,6–8]). In this form, consideration can also be given to the development of tensile fractures normal to the joints if some stepping is required for failure to occur (Fig. 2). However, these treatments only address the question of joint persistence and not necessarily the progressive development of the failure plane. Barton [9] refined these procedures by including the division of the planar rock mass into slices and the calculation of failure depth based on the concept of unstable excess (i.e. whereby excess forces are transferred from overstressed slices/blocks to underlying blocks). In this sense, the calculation considers sliding along portions of all overstressed joints, stepping down progressively from one joint to the next immediately beneath [9].

The question of joint continuity/persistence was further addressed by Einstein et al. [3] who developed probabilistic persistence models using a method of slices approach together with Monte Carlo simulations to express rock slope failure probability as a function of joint geometry and intact rock and joint resistance. In a similar fashion, stochastic modelling of discontinuity geometries has been used to assess kinematic feasibility and kinetic stability of rock slopes based on the clustering and connectivity of natural joint systems [10]. Such studies demonstrate the importance of discontinuity geometries, persistence, connectivity and clustering, as well as their statistical distribution, in forming a potential failure plane, but are still limited with regard to reproducing the progressive nature of the failure surface's development.

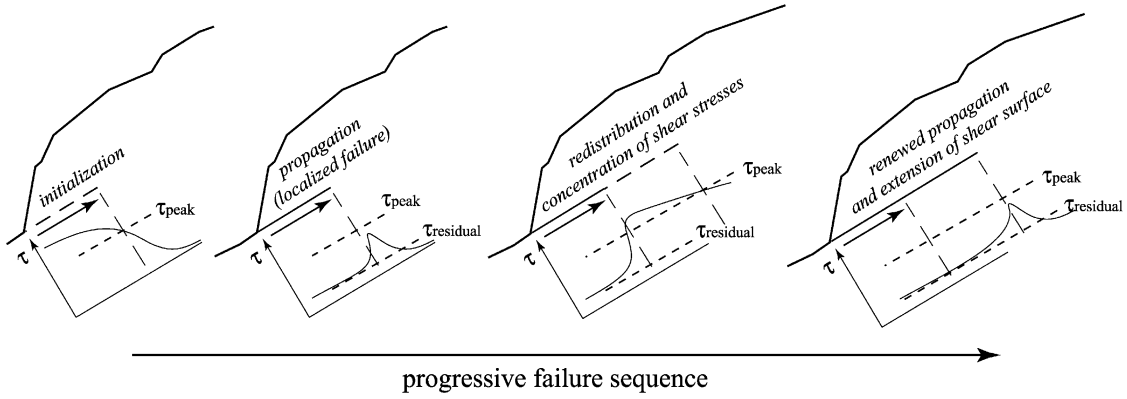

Fig. 1. Shear surface development through progressive failure (after Bjerrum [5]).

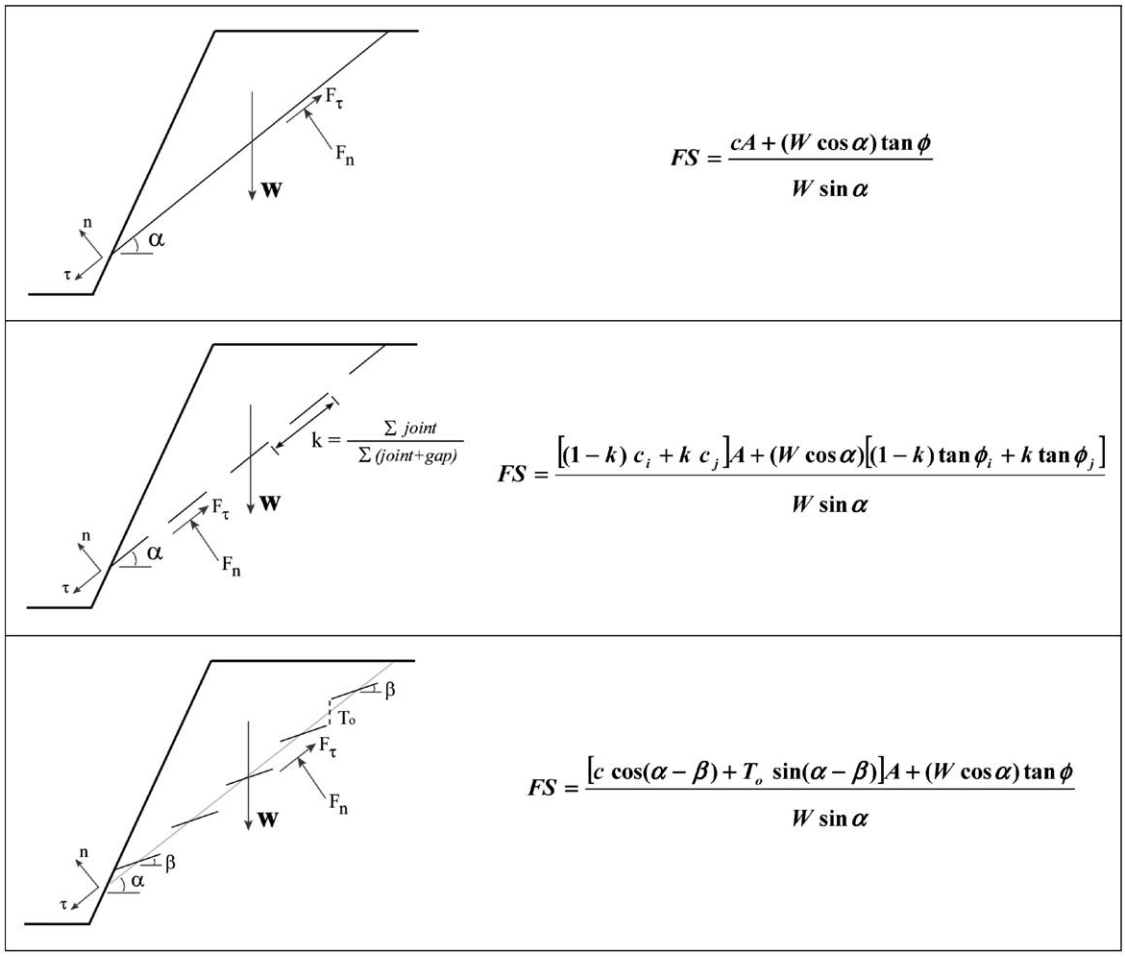

Fig. 2. Force-balance limit equilibrium solutions for planar-type failures, where: FS is the factor of safety, c and ϕ the cohesion and friction along failure surface, c_i and ϕ_i the cohesion and friction of intact rock, c_j and ϕ_j the joint cohesion and joint friction, A the surface area of failure (incorporating 2-D assumption of unit width), W the sliding rock mass weight, α the slope of failure plane, k the coefficient of continuity (after Jennings [7]), T_0 the intact tensile strength; and β is the angle of discontinuity in step path (after Jaeger [8]).

The key to progressive failure in rock slopes is that the process is predominantly driven by the propagation of fractures through intact rock between existing discontinuities. To consider these processes, several studies have adopted fracture mechanics principles to model the extension and development of a shear plane through a network of existing discontinuities. For example, Scavia [11] used the displacement discontinuity method to model the linear elastic stress intensity factors at the tips of a series of joints from which propagating cracks could extend and coalesce with neighbouring joints resulting in the development of a continuous failure plane (Fig. 3a). Kaneko et al. [12] also used the displacement discontinuity method and fracture mechanics' principles to model the progressive development of a shear plane, but differed in that pre-existing discontinuities were not included (i.e. the rock slope was assumed to be homogeneous). As such, stress concentrations arising at the toe of the slope were used to model the initiation and development of a shear plane upwards through the slope. However, Kaneko's models incorrectly predict the upper path of the failure plane near the head of the slope where tension cracks would normally develop, predicting instead a failure plane that curves from the toe to the upper face of the slope (Fig. 3b).

This is largely due to the fact that internal deformation and dilation are not considered, a limitation that generally applies to the above-mentioned analyses where only the processes acting along the developing shear plane are treated. Under such conditions, failure should initiate at the toe of the rock slope where the stresses are highest and propagate upwards. Such a failure mode would be considered as being predominantly brittle with very little internal deformation required to accommodate failure. Yet in many cases surface tension cracks appear at the top of the slope long before catastrophic failure occurs suggesting that failure is also partly driven through internal deformation mechanisms and dilation. These differences are depicted in Fig. 4, where the primary controls contributing to massive rock slope

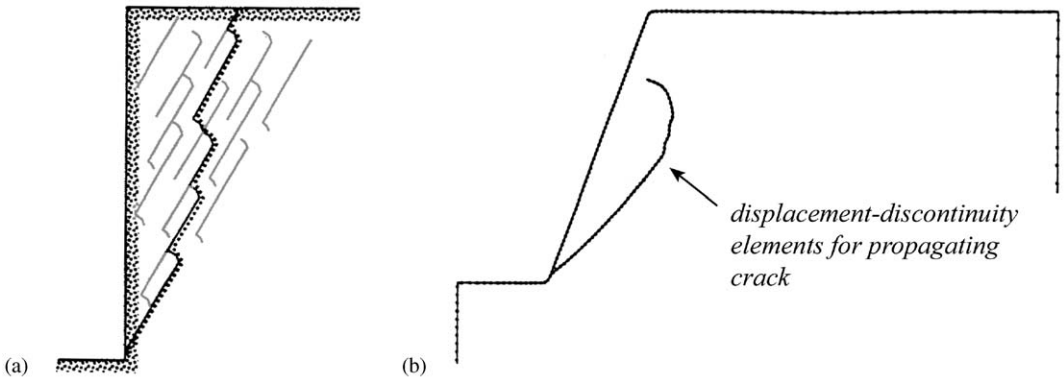

Fig. 3. Displacement–discontinuity modelling of shear surface development based on linear elastic fracture mechanics: (a) between natural discontinuities acting as stress concentrators (after Scavia [11]); and (b) through a homogeneous slope (after Kaneko et al. [12]).

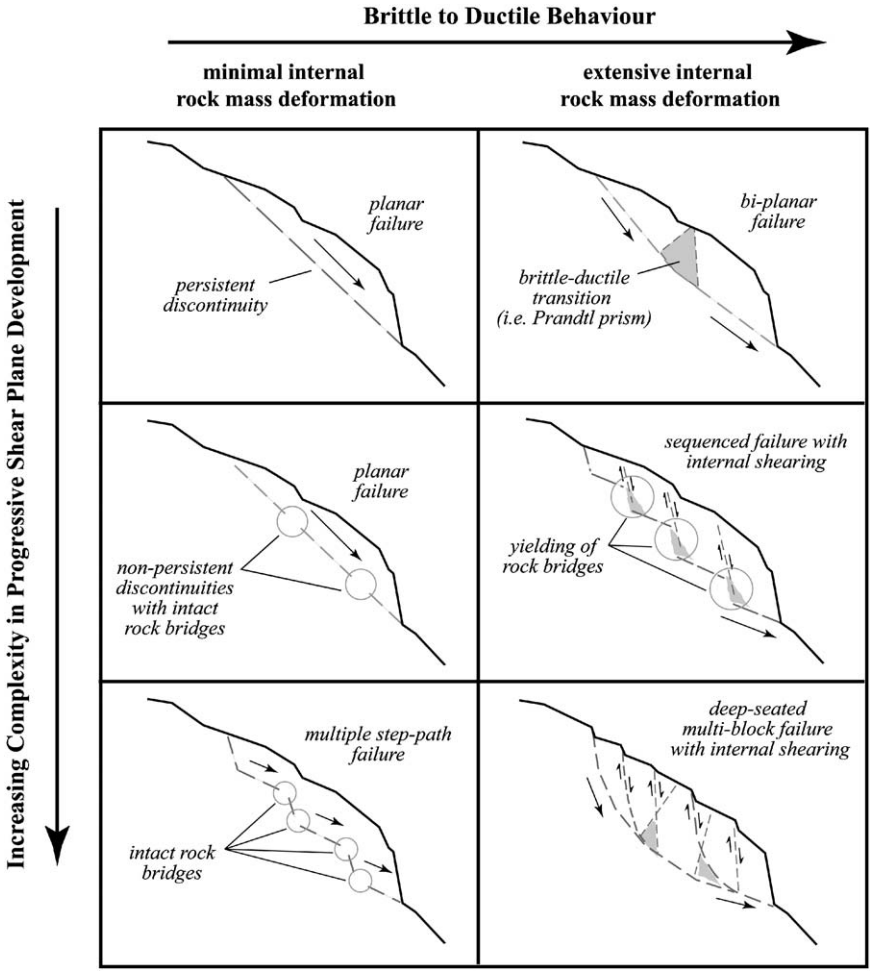

Fig. 4. Massive rock slope sliding mechanisms as controlled by progressive shear plane development and internal rock mass deformation/damage.

failure can be viewed as strength degradation in the form of shear plane development (i.e. progressive failure) and strength degradation manifested through internal slide mass deformation and damage mechanisms.

Depending on the complexity of the rock mass geology and subsurface structure, these controls will vary in their influence on the overall stability state. In cases where adversely oriented discontinuities are relatively persistent and/or failure only requires the propagation of a shear plane through intact rock bridges, the failure mechanism will kinematically require very little internal deformation/damage for

release (Fig. 4, left-hand column). Examples from the Alps include the 1806 Goldau slide, where failure occurred along a shear surface parallel to planar bedding contacts, and the 1881 Elm slide, where failure was initiated by undermining of the slope (Fig. 5).

If kinematic release does not occur along one or more relatively dominant planar features, failure requires internal deformation of the rock mass whereby the slide body undergoes a brittle to ductile transition as damage accumulates, localized slip along joints occurs and rock mass strength degrades (Fig. 4, right-hand column). An Alpine example of this type includes the 1963 Vaiont slide, where Mencl [14] proposed the development of an internal damage zone (referred to as a Prandtl wedge) to explain failure along bi-planar slip surfaces (Fig. 6). Limit equilibrium techniques have long recognized the importance of internal shears to properly take into account the kinematics of sliding blocks (e.g. [15]). As such, Martin and Kaiser [16] showed that these internal shears, and the internal distortions that occur along them, are necessary in certain modes of rock slope instability to accommodate motion along a basal slip surface.

2.2. The 1991 Randa rockslide

Situated in the Matter Valley in the southwestern Swiss Alps, the 1991 Randa rockslide involved the failure of 30 million m^3 of massive crystalline rock (Fig. 7). The slide occurred in two distinct episodes with the first slide occurring on April 18, 1991 and the second on May 9, 1991. The volumes of these individual events were approximated as 20 and 10 million m^3, respectively [17]. Damage resulting from the two events included the destruction of the main road and rail line along the valley (which provides access to the resort town of Zermatt and the Matterhorn), and the damming of the Vispa River and the subsequent flooding of the town of Randa [18].

The failed rock included massive gneisses alternating with mica-rich paragneisses (Fig. 7) belonging to the Penninic St. Bernhard nappe. As foliation dips favourably into the slope, Schindler et al. [19] suggested that failure occurred along extensive shallow dipping stress-relief joints parallel to the surface. These joints can be inferred along the sliding surface but are limited in persistence when encountered in surface outcrops [20]. A series of steep sub-vertical faults were also proposed as dividing the slide mass into smaller units [17,19], presumably to explain the episodic nature of the slide.

Analysis of climatic and regional seismic data showed no clear indications of a triggering event [19]. Although no explicit triggering mechanism could be resolved, Schindler et al. [19] noted that failure coincided with a period of heavy snowmelt. However, examination of snow height, precipitation and temperature records shows that this was not an exceptional event and that heavier snowmelts had been recorded in previous years (Fig. 8; [4]). Eberhardt et al. [4] instead suggest that time-dependent mechanisms relating to brittle strength degradation and progressive failure may more likely be the significant contributing factors that brought the slope to failure. Similar hypotheses were proposed in the

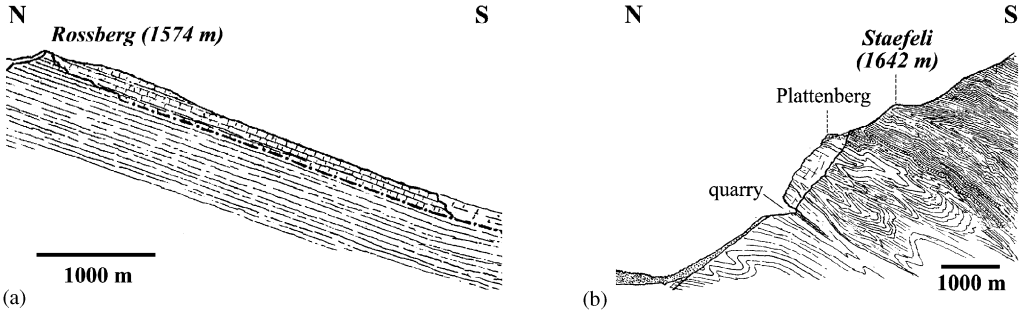

Fig. 5. Schematic cross-sections of the (a) Goldau and (b) Elm rockslides in Switzerland (after Heim [13]).

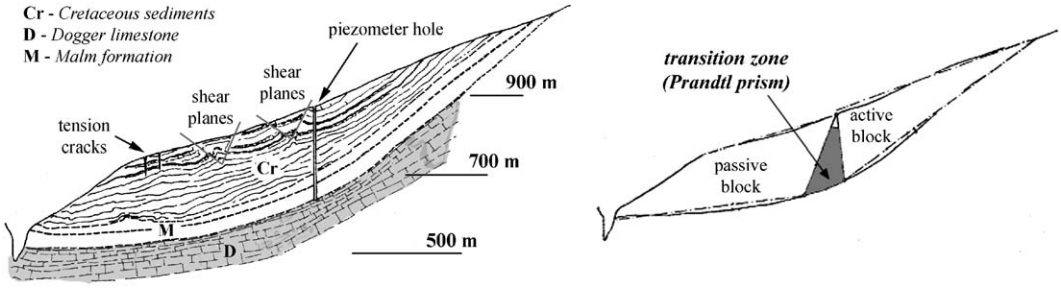

Fig. 6. Schematic cross-section of the Vaiont slide showing transitory yield zone development in the form of a Prandtl prism (after Mencl [14]).

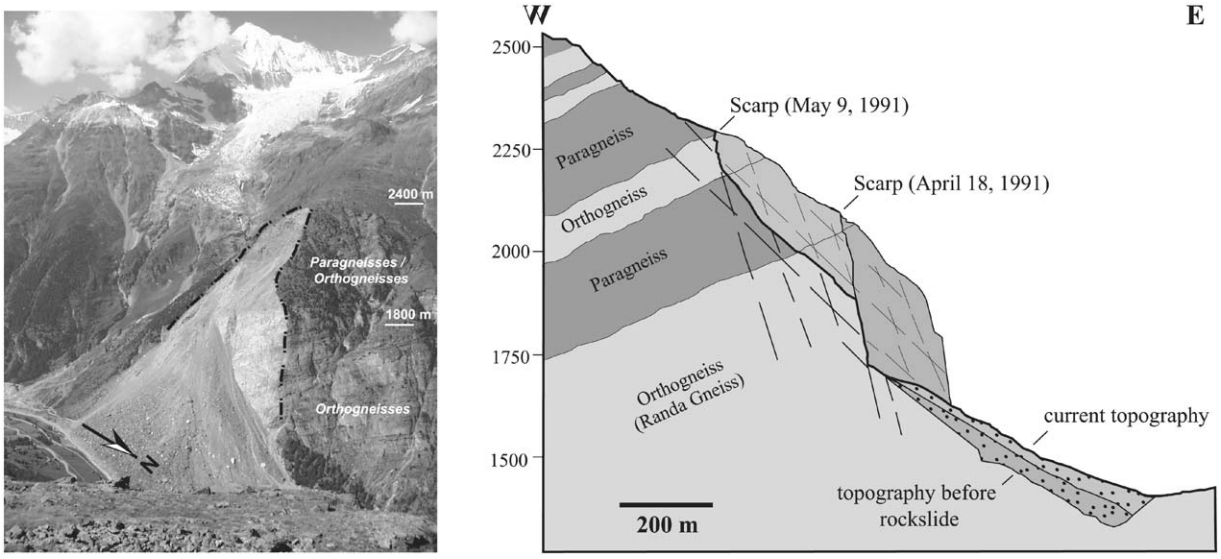

Fig. 7. Photo of the 1991 Randa rockslide and cross-sectional illustration showing the two key sliding events (photo provided by H. Willenberg; cross-section modified after Schindler et al. [19]).

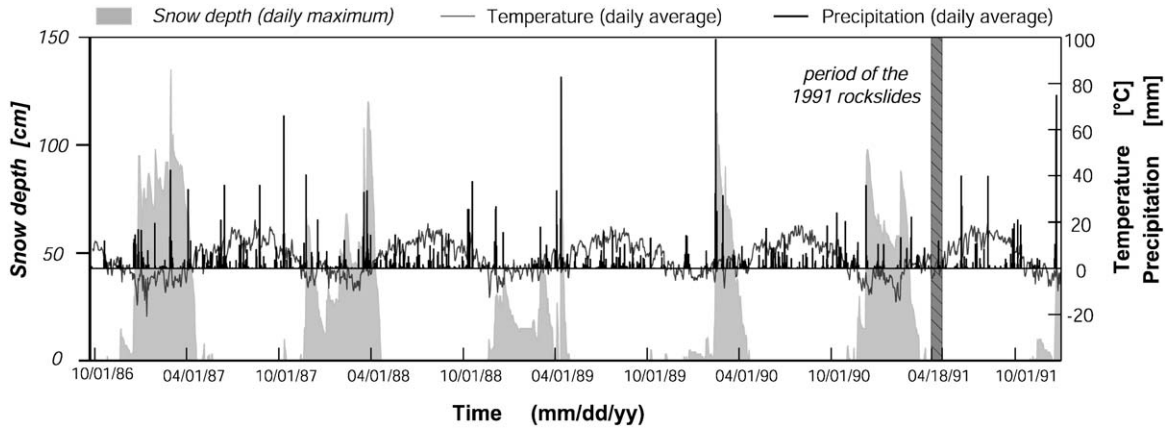

Fig. 8. Snow depth, temperature and precipitation records for Zermatt climate station near the Randa rockslide (after Eberhardt et al. [4]; data provided by MeteoSchweiz).

case of another natural rockslide in gneissic rock at Pandemonium Creek in western Canada, where again no anomalous event could be identified as a trigger and the gradual long-term reduction in rock mass strength was suggested as a possible cause [21].

3. Numerical analysis of initiation and progressive failure

3.1. Methodology and techniques adopted

Limit equilibrium and numerical analysis techniques have specific advantages and disadvantages inherent in their respective methodologies. These are reviewed in detail with respect to their application to rock slope analyses by Stead et al. [22]. As discussed in the previous section, certain rock slope failures can be largely kinematically controlled and treated as a limit equilibrium problem. Diverging from a phenomenological approach though, and thinking mechanistically, most unstable rock slopes undergo some degree of progressive shear plane development, deformation and extensive internal disruption of the slope mass. As a consequence, the factors governing initiation and eventual failure are complex and not easily included in simple static analyses.

In contrast, numerical methods are able to provide approximate solutions to problems, which otherwise would not be solvable using limit equilibrium techniques alone. This permits the treatment of rock slope stability problems involving complexities relating to geometry, material anisotropy, non-linear behaviour, the inclusion

of in situ stresses and the presence of coupled processes (e.g. pore pressures, seismic loading, etc.). Numerical techniques used for rock slope analyses are generally divided into continuum and discontinuum approaches, or when combined, hybrid approaches [22].

Continuum approaches used in slope stability analysis include the finite-difference and finite-element methods. In both these methods the problem domain is divided (discretized) into a set of sub-domains or elements (Fig. 9a). A solution procedure may then be based on numerical approximations of the governing equations, i.e. the differential equations of equilibrium, the strain–displacement relations and the stress–strain equations, as in the case of the finite-difference method (FDM). Alternatively, the procedure may exploit approximations to the connectivity of elements, and continuity of displacements and stresses between elements, as in the finite-element method (FEM). In this study both methods were used interchangeably where a continuum approach proved favourable, depending on specific features available in the adopted commercial codes: FEM-VISAGE [23]; FDM-FLAC [24].

Discontinuum methods (e.g. discrete-element, distinct-element) treat the problem domain as an assemblage of distinct, interacting bodies or blocks that are subjected to external loads and are expected to undergo significant motion with time. Algorithms generally use a force–displacement law to specify the interaction between deformable intact rock blocks and a law of motion, which determines displacements induced in the blocks by out-of-balance forces. Joints are viewed as interfaces between the blocks and are treated as a boundary condition rather than a special element in the model. Block deformability is introduced through the discretization of the blocks into internal constant-strain elements (Fig. 9b). The dual nature of these discontinuum codes make them particularly well suited to rock slope instability problems: they are capable of simulating large displacements due to slip, or opening, along discontinuities; and they are capable of modelling the deformation and material yielding of the joint-bounded intact rock blocks, which is particularly relevant for high slopes in weak rock and for complex modes of rock slope failure [25]. Where a discontinuum approach proved favourable, the commercial distinct-element code UDEC [26] was used.

Although both continuum and discontinuum analyses provide useful means to analyse rock slope stability problems, complex failures like Randa involve an added complexity relating to both interactions along existing discontinuities and the creation of new ones through brittle fracturing of intact rock. To treat these problems, new developments in hybrid finite-/discrete-element codes were utilized and applied, which allow for the modelling of both intact rock behaviour and the development of fractures [27]. In this case, the commercial code ELFEN [28] was used.

Starting from a continuum representation of the solid material by finite elements, fracturing in ELFEN is controlled according to a fracturing criterion specified through a constitutive model (e.g. Rankine tension, rotating crack, Mohr–Coulomb, etc.). At some point in the analysis the adopted constitutive model predicts the formation of a failure band within a single element or between elements. The load carrying capacity across such localized bands decreases to zero as damage increases until eventually the energy needed to form a discrete fracture is released. At this point the topology of the mesh is updated, initially leading to fracture propagation within a continuum and eventually resulting in the formation of a discrete element as the rock fragments (Fig. 10).

Subsequent motion of these discrete elements and further fracturing of both the remaining continuum and

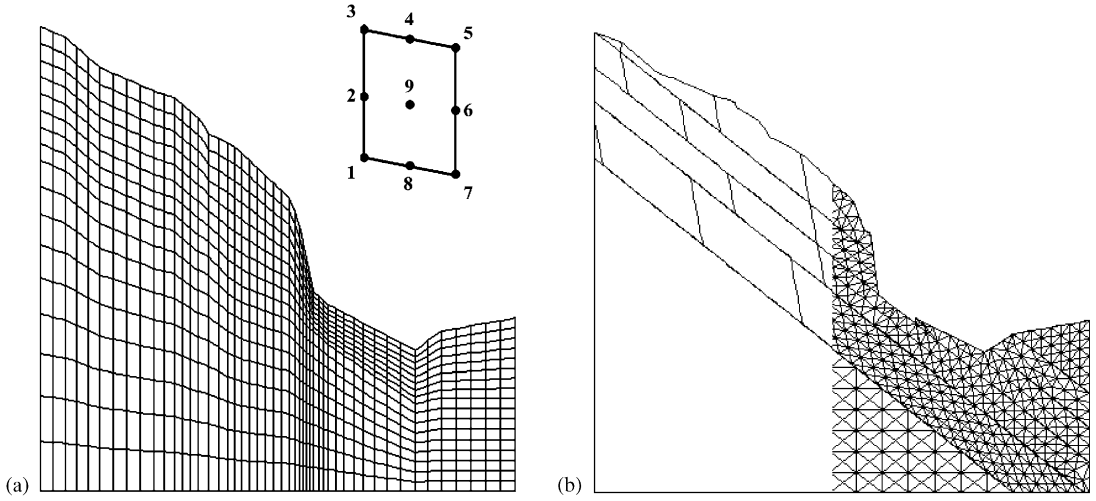

Fig. 9. (a) Continuum and (b) discontinuum numerical methods, showing models based on the 1991 Randa rockslide.

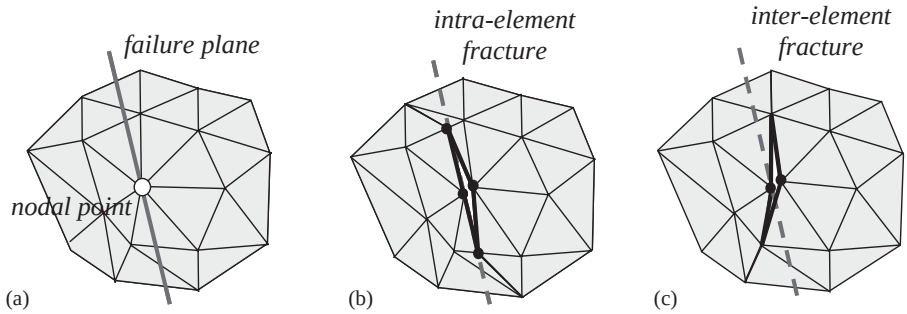

Fig. 10. ELFEN crack insertion procedure showing: (a) initial configuration; and (b) crack development through element; or (c) crack development along element boundary (after Yu [29]).

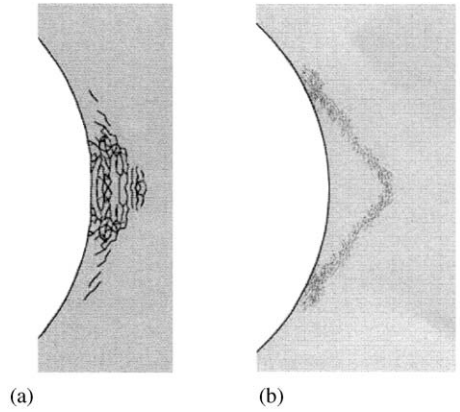

Fig. 11. Hybrid finite-/discrete-element modelling (ELFEN) of: (a) tensile axial splitting (Lac Du Bonnet Granite); and (b) shear failure development, for borehole breakout modelling of different rock types (Cardova Cream Limestone) (after Klerck [30]).

Table 1
Material properties for Randa continuum and hybrid models

Parameter		Randa gneiss		Glacial ice
Young's modulus (GPa)		30		10
Poisson's ratio		0.33		0.30
Density (kg/m^3)		2600		900
	Initial state	Damage state 1	Damage state 2	
Cohesion (MPa)	10	1.0	0.1	—
Internal friction (deg)	5	20	40	—
Tensile strength (MPa)	1.0	0.1	0	—
Strain energy release rate (N/m)		200		

previously created discrete elements is then simulated. This evolution process is continued until either the system comes to equilibrium or up to the time of interest. Klerck [30] and Crook et al. [31], when modelling borehole breakout, showed that by augmenting the standard Mohr–Coulomb yield function with a Rankine tensile cutoff, thereby coupling tensile and shear damage, they were able to effectively model both brittle tensile axial splitting fractures and more ductile shear features (Fig. 11). For the shear-type features, the fracture process was wholly extensional resulting in the development of en echelon cracks that originate at the borehole wall and propagate at an angle and intersect at some distance away from the borehole wall. The cracks form as a result of inelastic extensional strain associated with dilation. By applying such techniques, it becomes possible to model both the behaviour of a continuum and a discontinuum, and the transformation of the rock mass from a continuum to a discontinuum (Fig. 11).

3.2. Modelling of process initiation

Initial 2-D finite-element modelling was performed to examine the natural stress state for the unstable 1991 Randa slope mass based primarily on its topographic profile. The model incorporated nine-noded quadrilateral elements, and several model geometries were tested to determine the extent at which boundary effects were negligible. Stresses were initialized assuming a horizontal to vertical stress ratio of 0.5 (i.e. $K = \sigma_H/\sigma_V = 0.5$), but model results were also tested for $K = 1$ and 2. Initial models assumed a homogeneous, isotropic rock mass (input values are given in Table 1) without the inclusion of pore pressures. As such, the methodology adopted was to start simple and build-up the complexity as required.

Results from this analysis (Fig. 12), reveal that the rounded corner formed by the transition of the steep rock slope face to the valley floor acts as a natural stress concentrator. The sharpness of this stress concentration depends on the initial in situ stress state and is sharpest, in relation to the vicinity of the toe of the 1991 Randa slope failure, when the initial vertical stress is twice that of the horizontal stress ($K = 0.5$). In examining complex rock slope failure mechanisms, Stead et al. [32] demonstrated that the initial in situ stress ratio is an important input parameter that is commonly overlooked, and Chowdhury [33] suggested that the initial

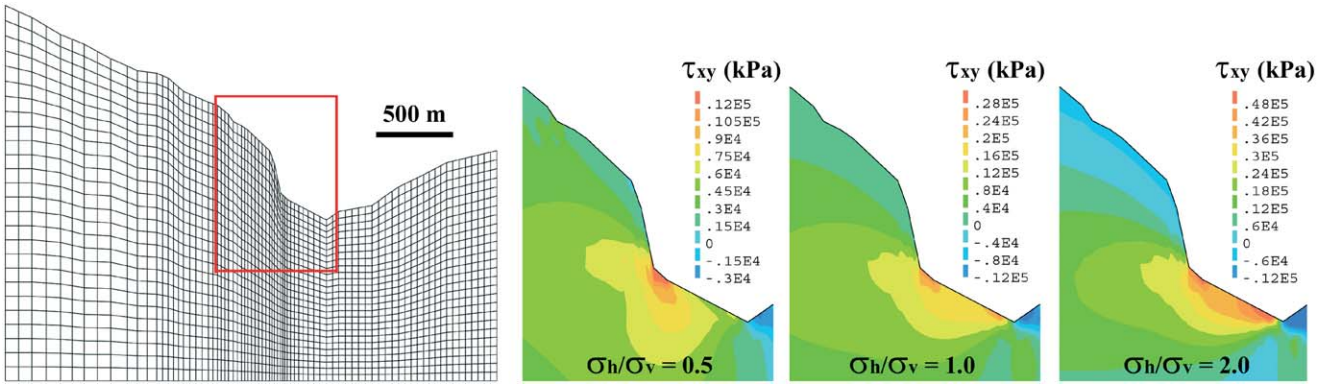

Fig. 12. Finite-element continuum modelling based on the Randa rock slope profile prior to failure, showing shear stress concentrations for three different vertical to horizontal initial in situ stress ratios.

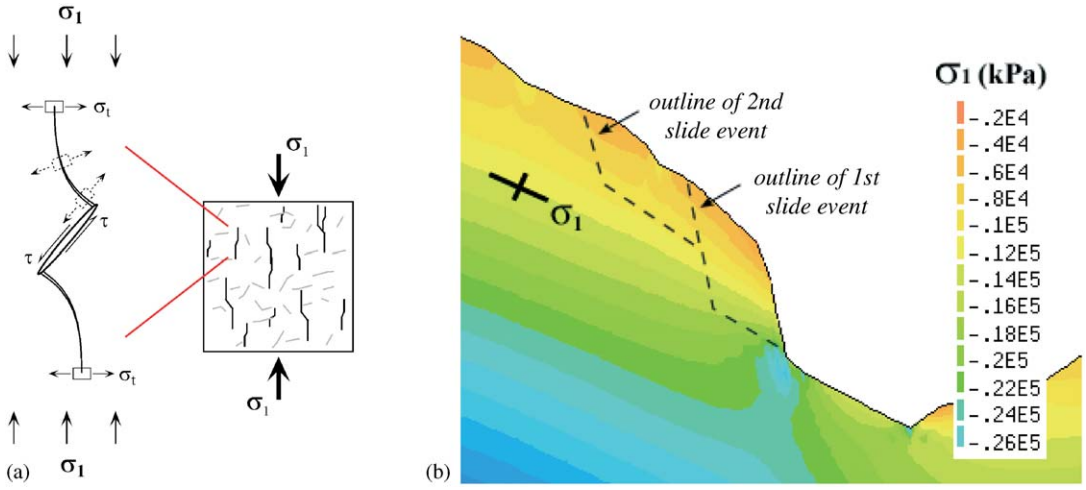

Fig. 13. (a) Illustration of fracture propagation from tips of critically stressed discontinuities (i.e. Griffith cracks) in the direction of the major principal stress (σ_1); (b) approximate outline of the two Randa rockslide events superimposed over the finite-element σ_1 stress contours.

stress state controls the direction in which the failure surface propagates. Results presented in Fig. 12 show that as the K ratio increases and the horizontal stress exceeds the vertical component (i.e. the initial alignment of the maximum principal stress, σ_1, changes from sub-vertical to sub-horizontal), the shear stress concentration becomes more evenly distributed along the valley floor. Although the overall shear stress magnitude increases, the important factor is the alignment of the maximum principal stress, σ_1, relative to the problem geometry in terms of the propagation of the shear plane.

Apart from varying the K ratio through several different test models, an initial stress ratio of $K = 0.5$ was adopted throughout most of the study. This is in approximate agreement with inversion results from Kastrup et al. [34] based on fault plane solutions of seismic events recorded in the region, suggesting an extensional regime with a vertical stress component greater than the horizontal (i.e. $K < 1.0$). The corresponding shear stress distribution shown in Fig. 12 (for $K = 0.5$) likewise corresponds to the location of the toe of the 1991 Randa failure surface, and it would be within this zone that the process of progressive failure potentially initiated. The initiation and development of the sliding surface would then depend on the presence and geometrical configuration of discontinuities within the critically stressed toe region. The basic tenets of fracture mechanics show that when such discontinuities (or flaws) are critically aligned with respect to the direction of loading and the deviatoric stress concentrations at their tips exceed the strength of the material, fracture propagation will occur in a plane normal to the minor principal stress, σ_3, i.e. parallel to the maximum principal stress, σ_1; Fig. 13a [35–37]. In the case of a slope, which represents a free surface, σ_1 will be parallel to topography. Given the coincidence of the base of the Randa rockslide failure surface parallel to topography (Fig. 13b shows this with respect to the σ_1 stress contours), the role of brittle fracture processes would seem significant.

Accordingly, the orientation of discontinuities that would most favourably contribute to shear plane

initiation and development would be those aligned sub-parallel to topography. As previously noted, field observations do suggest the presence of stress-relief joints sub-parallel to the surface at Randa even though foliation, and the dominant joint set associated with it, dips favourably sub-perpendicular into the slope [4,19]. Stress-relief or "sheet" joints parallel to topographic surfaces are characteristic of crystalline rock masses and are generally accepted to be the result of rock dilation due to unloading effects. Although their origin and genesis may be partly disputed (i.e. preglacial or glacial), evidence of stress-relief jointing sub-parallel to glaciated valley walls confirms that rapid glacial erosion is sufficient to produce sheet structures in crystalline rock [38]. Thus it would seem reasonable that the initiation of progressive failure in natural rock slopes could be in part related to glacial processes (i.e. glacial loading, retreat, rebound, etc.), as these processes generally represent the last major large-scale change to the slope's equilibrium condition.

The next series of finite-element models analysed were therefore used to investigate the role glacial processes may have played in the initiation and development of the initial conditions for progressive failure at Randa. Glacial unloading was simulated assuming the glacial erosion of approximately 2000 m of rock relative to the valley bottom (Fig. 14). This value is in accordance with glacial ice surface maximums reconstructed for the last glaciation in the Central Swiss Alps [39]. Material properties were based on those for glacial ice [40] and the Randa gneiss (Table 1). To model damage initiation, a Mohr–Coulomb elasto-plastic yield criterion was used (with the corresponding c and ϕ values listed in Table 1 under "initial state"). In modelling rebound-induced damage, the key controlling mechanism involves the release of strain energy leading to the generation of tensile extensional fractures. Hence, tensile damage is the key-modelling indicator, which in turn is a function of the tensile strength. The process of glacial rebound was modelled in several stages to include the glacial erosion of rock material to shape the valley, its replacement by glacial ice, and the retreat of the glacier from the valley (Fig. 14).

Modelling results demonstrate that based on the given assumptions regarding maximum glacier height (i.e. 2000 m above the valley bottom), tensile fracture damage parallel to topography can be induced through glacial unloading/rebound. Initial sensitivity analyses showed that tensile damage developed at the toe of the Randa slope but only for tensile strengths less than 1 MPa. It should be noted though that these models were run without the inclusion of pore pressures thereby requiring lower values of tensile strength for damage to initiate. When pore pressures were added, the extent of tensile damage increased considerably (Fig. 15) and allowed tensile strength values more representative of an

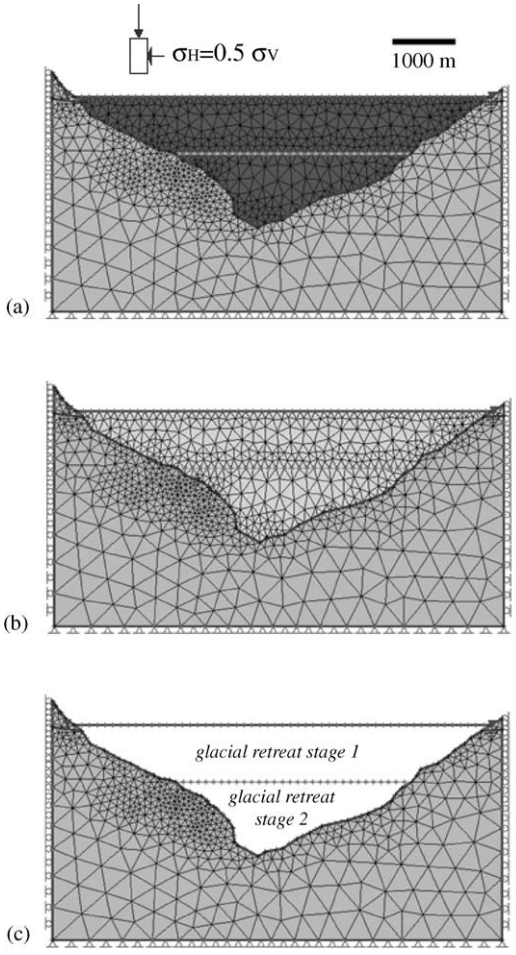

Fig. 14. Finite-element continuum modelling of glacial loading and unloading processes, showing simulation stages which include: (a) initial bedrock conditions; (b) shaping of the valley through glaciation and the replacement of rock by glacial ice; and (c) the retreat of the glacier from the valley in two stages.

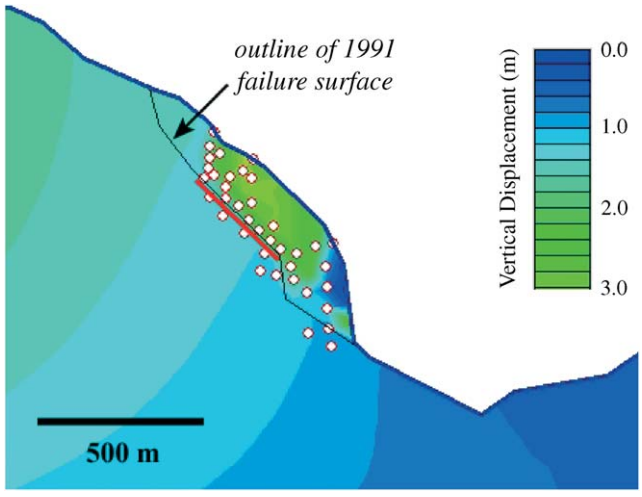

Fig. 15. Finite-element continuum modelling of starting conditions for progressive failure showing tensile damage indicators generated during simulation of glacial unloading. Note linear trend of tensile damage indicators coinciding with upper portion of the 1991 Randa failure surface (marked in red).

undamaged gneissic rock mass to be used (in this case, 2.5 MPa). The water table was approximated as being just below the glacier–bedrock contact. Interestingly, these results show that the tensile damage approximately coincides with the outline of the 1991 Randa rockslide, most notably in the upper section where linear trends between the tensile damage indicators and observed failure surface overlap (highlighted in red in Fig. 15). Together, these model results suggest that (1) the development of tensile fracture damage preferentially oriented sub-parallel to topography following glacial unloading, combined with (2) shear stress concentrations induced through oversteepening of the valley walls, provide a likely initiation source for progressive shear plane development.

3.3. Modelling of shear plane development

The modelling of progressive shear plane development is somewhat more challenging as the model needs to incorporate both strength degradation (as plastic shear strains evolve and/or tensile fracture damage develops), and ideally, brittle fracture propagation and its temporal evolution. On a simpler more practical level, strength degradation can be easily implemented as a function of strain through the use of continuum techniques. Hajiabdolmajid and Kaiser [41] demonstrated this by modelling cohesion loss as a function of plastic strain in a back analysis of the 1905 Frank Slide in Canada. As cohesion is destroyed, the frictional component of strength begins to mobilize (Fig. 16).

Fig. 17 provides an extension of the finite-element models shown in Fig. 12 to examine shear plane development at Randa as a function of rock mass strength degradation using a Mohr–Coulomb elasto-plastic yield criterion. Strength values were initially set to those for a generally coherent gneissic rock mass and then altered, with the rock mass strength progressively decreasing as a function of increasing brittle fracture damage (Table 1). Fig. 17 demonstrates the transition from stable slope conditions to those of shear failure by showing the evolution of shear strains and horizontal displacements over the last two stages of progressive failure. Similar to back-calculated limit equilibrium values [42], failure occurs when the cohesion decreases to 1.0 MPa (i.e. ~90% reduction in assumed rock mass cohesive strength). Examination of the 2-D finite-element results with respect to the actual shape of the failure surface shows that although the lower section of the yield surface agrees closely, the upper section appears to extend further back beyond the observed failure back-scarp (Fig. 17). Interestingly, several deep active tension cracks can be found in this upper slope region, which are currently being monitored as part of an on-going investigation relating to present-day rockslide activity [20].

These results demonstrate that continuum modelling can be used to examine the evolution of stresses, strains and plastic yielding within the rock mass during the formation of a slide surface. However, it should be emphasized that it does so based on a simplified representation of rock mass strength degradation over an equivalent continuum that incorporates both intact rock and discontinuity effects (i.e. a representative element volume). Another option may then be to examine aspects of progressive failure through the adoption of a discontinuum technique. Examples of strength-reducing factors specific to discontinuities include the loss of cohesive strength as remnant intact rock bridges along the shear plane are destroyed, and

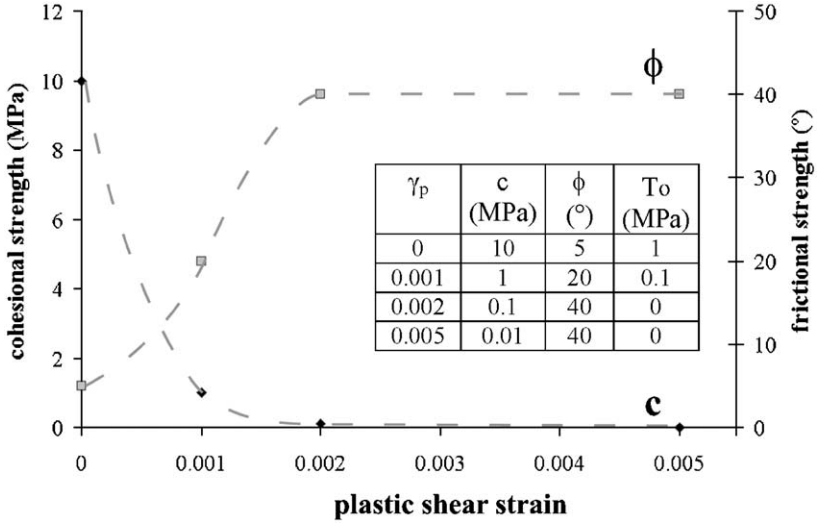

γ_p	c (MPa)	ϕ (°)	To (MPa)
0	10	5	1
0.001	1	20	0.1
0.002	0.1	40	0
0.005	0.01	40	0

Fig. 16. Decreasing cohesive strength (c) and the corresponding increase in the mobilized frictional strength component (ϕ) due to increasing brittle fracture damage, in this example defined as a function of plastic shear strain (γ_p) as approximated from mechanistic-based uniaxial compression damage testing of granitic rocks [43]. Note that T_0 refers to tensile strength.

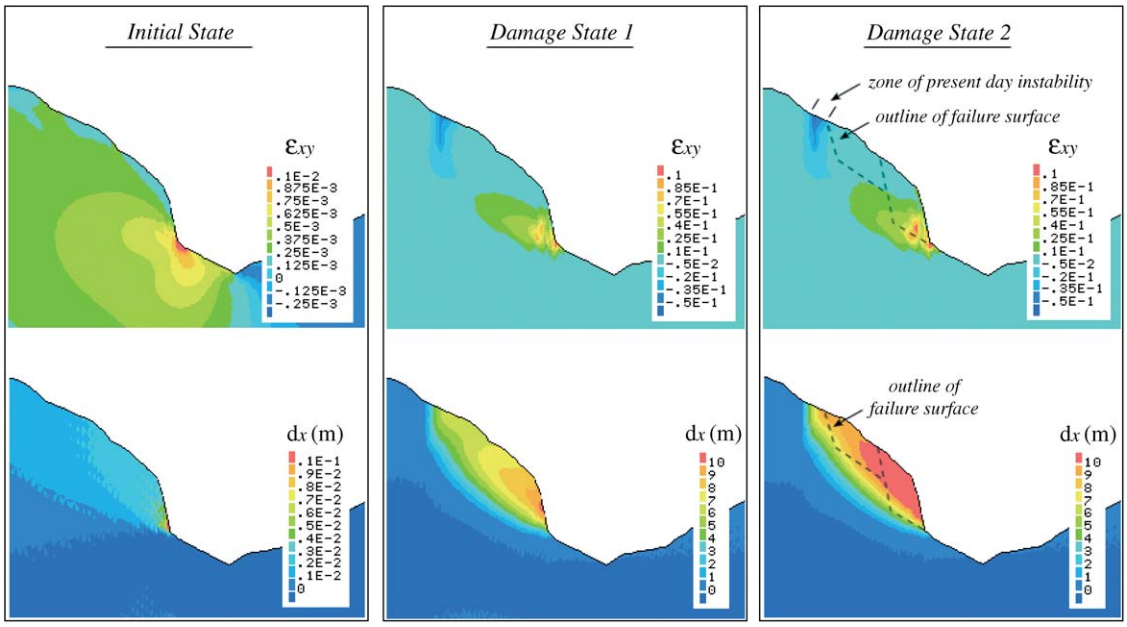

Fig. 17. Evolution of shear strains (ε_{xy}) and horizontal displacements (d_x) over three stages of progressive rock mass strength degradation (see Table 1) leading to catastrophic slope failure. The dashed line corresponds to the outline of the 1991 Randa slide surface.

reductions in frictional strength as interlocking asperities along the discontinuity surfaces are sheared during mobilization (Fig. 18). To incorporate these effects, discontinuum techniques like the distinct-element method can be applied.

Fig. 19 presents a distinct-element analysis of the 1991 Randa rockslide in which discontinuity strengths were modelled as progressively decreasing (Table 2). One limiting assumption required by the distinct-element method is the inclusion of fully persistent, interconnected discontinuities. This condition would be most applicable at the stage in the progressive failure process where a significant portion of the shear surface has already developed. For the analysis performed, two discontinuity sets were included—those dipping at an angle of 50° out of slope, corresponding to the topography-parallel stress-relief jointing, and one subvertical set as suggested by Schindler et al. [19] (Fig. 7). Based on this conceptualization, the distinct-element analysis was carried out assuming an initial joint friction of 40° and joint cohesion of 5 MPa (representing the strength provided by intact rock bridges). Models then simulated progressive failure through gradual reduction of joint cohesion (Table 2) using a methodology similar to that applied for the continuum models presented in the previous section. Results indicate that the failure process initiates when the joint cohesion is reduced to 1 MPa, and that catastrophic failure occurs when the joint cohesion approaches 0.1 MPa (Fig. 19). It can be noted that these critical cohesive strength thresholds are similar to those obtained for the continuum models.

Both the continuum and discontinuum models show that their formulations can capture certain aspects of progressive shear plane development. Notwithstanding, they are still limited in terms of modelling key processes related to brittle fracture initiation and propagation. As such, modelling was extended to include the use of hybrid finite-/discrete-element modelling techniques. Two constitutive fracture models were adopted and compared, the first favouring the development of a "shear failure" (combined Mohr–Coulomb/Rankine crack model) and the second favouring tensile fractures (Rankine crack model). The basic material properties used were kept the same as those given in Tables 1 and 2 (i.e. for the finite-element continuum and discrete-element discontinuum, respectively). Results are provided in Figs. 20 and 21.

Comparisons between the two different constitutive models show that the shear-based Mohr–Coulomb fracture constitutive model reproduces the dimensions of the 1991 Randa slide mass very well using the c and ϕ values listed under "Damage State 1" in Table 1 (Fig. 20). In doing so, the influence of the shear constitutive fracture model can be fully appreciated as shear stresses and strains induced through gravitational loading of the continuum drive the progressive development of the failure surface (e.g. compare Fig. 17 with Fig. 20). This leads to the formation of numerous subvertical tension/extension cracks (i.e. normal to the direction of downslope strains) through the Rankine tension cutoff, that together align to enable the formation of a shear plane sub-perpendicular to the tensile fractures (Fig. 20).

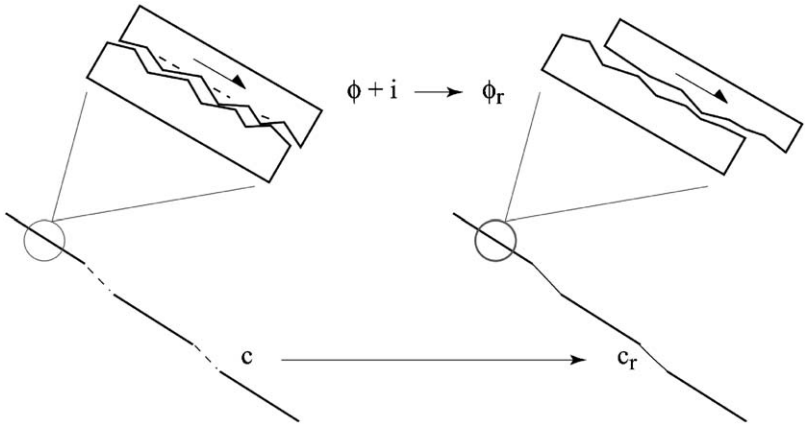

Fig. 18. Schematic illustration of shear strength degradation along a discontinuous shear surface involving loss of cohesion (c to c_r) and fictional strength ($\phi + i$ to ϕ_r) due to destruction of remnant intact rock bridges and interlocking discontinuity surface asperities, respectively.

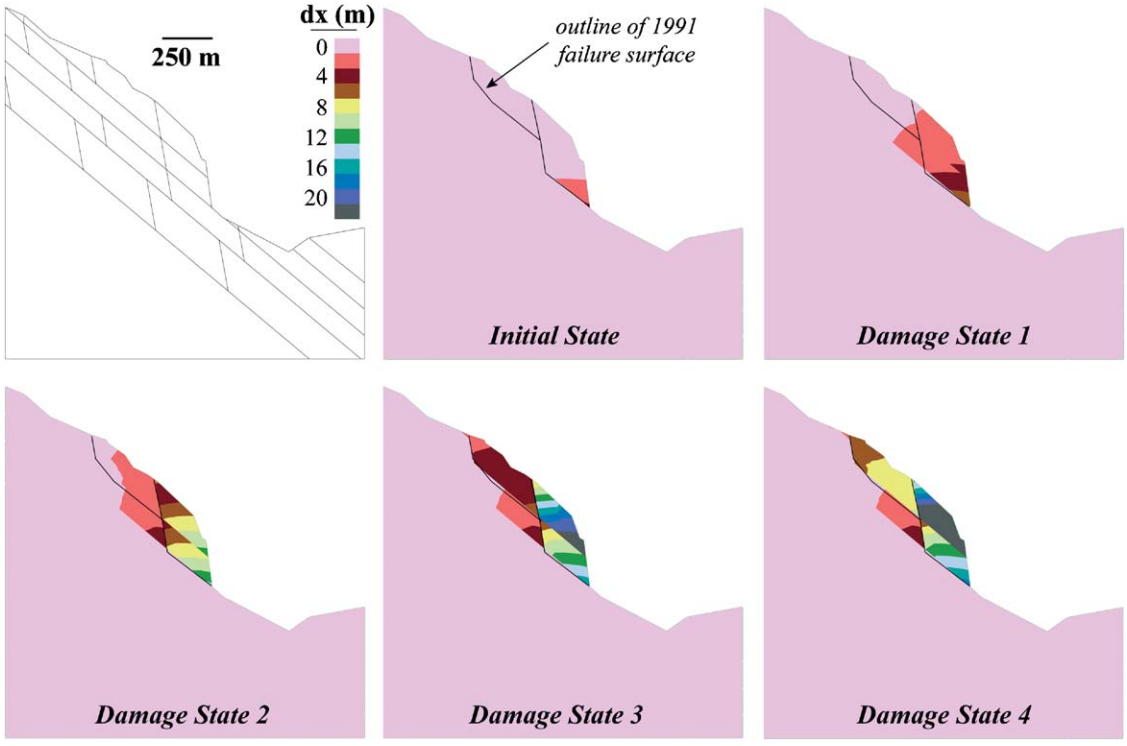

Fig. 19. Discontinuum modelling of progressive failure showing evolution of horizontal displacements over several stages of discontinuity strength degradation (in the form of joint cohesion reduction, as given in Table 2).

Similarly, results for the Rankine tensile constitutive fracture model reproduce the dimensions and irregular stepped nature of the Randa failure surface very well (Fig. 21). In contrast, though, these models favour the development of brittle tensile fracture propagation sub-parallel to the topography (i.e. parallel to σ_1). Shear along the failure surface, therefore, only becomes a factor after the failure surface is nearly fully developed and mobilization becomes possible. In other words, the failure surface only becomes a "shear" surface once tensile fracturing has progressed to the point where significant cohesion loss has occurred along the path of coalescing fractures and larger displacements become possible through kinematic feasibility and slide mass mobilization.

3.4. Internal deformation and staged failure

As suggested by the right-hand column in Fig. 4, the irregular nature of the Randa slide surface would necessitate the development of internal deformations to accommodate sliding. Martin and Kaiser [16] depict

Table 2
Material properties for Randa discontinuum and hybrid models

Parameter	Randa gneissic rock mass
Young's modulus (GPa)	30
Poisson's ratio	0.33
Density (kg/m^3)	2600
Cohesion (MPa)	10
Internal friction (deg)	5
Joint normal stiffness (GPa/m)	10
Joint shear stiffness (GPa/m)	1

	Initial state	Damage state 1	Damage state 2	Damage state 3	Damage state 4
Joint cohesion (MPa)	5.0	1	0.5	0.1	0
Joint friction (deg)	40	40	40	40	40

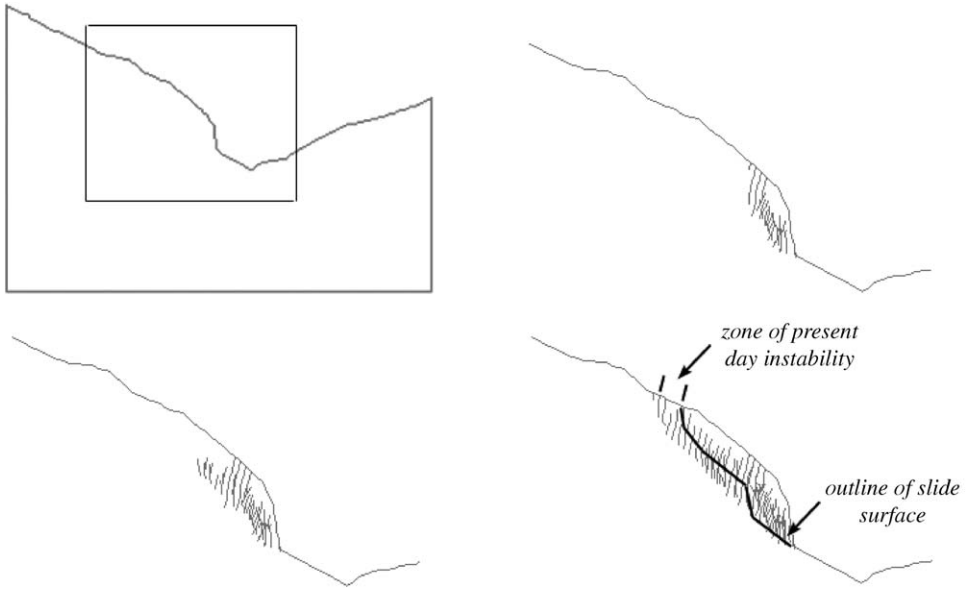

Fig. 20. Hybrid finite-/discrete-element model employing a Mohr–Coulomb shear fracture constitutive model, showing modelled progressive development of the slide surface relative to the 1991 Randa failure surface.

this process as localized yielding inside the slide mass to allow rigid body motion along an irregular slip surface. When the internal geology is influential, yielding may instead occur along pervasive internal shear zones [15,16]. Similar processes were also forwarded by Mencl [14] in the form of a Prandtl's wedge transition zone in which sliding along a bi-planar failure surface may be accommodated through internal slide mass yielding (Fig. 6).

The final series of numerical models investigated were thus directed towards exploring the contributing role of internal rock mass strength degradation, yielding and deformation with respect to the development of the Randa rockslide. In particular, these processes were analysed with respect to explaining the staged nature of the 1991 failure (i.e. incorporating the two key slide events illustrated in Fig. 7). Discontinuum techniques were first employed in this situation using the distinct-element method to model the rock slope failure as a Prandtl's wedge problem assuming a bi-planar failure surface that approximates the 1991 slide surface. Accordingly, emphasis was not placed on yielding along the failure surface but within the intact slide body itself. Terzaghi's [1] effective cohesion relationship was used to simulate the presence of intact rock bridges along the eventual failure surface.

By minimizing slip along the failure surface, a strain-softening criterion was used to simulate damage in the

Fig. 21. Hybrid finite-/discrete-element model employing a Rankine tensile fracture constitutive model, showing modelled progressive development of the slide surface relative to the 1991 Randa failure surface.

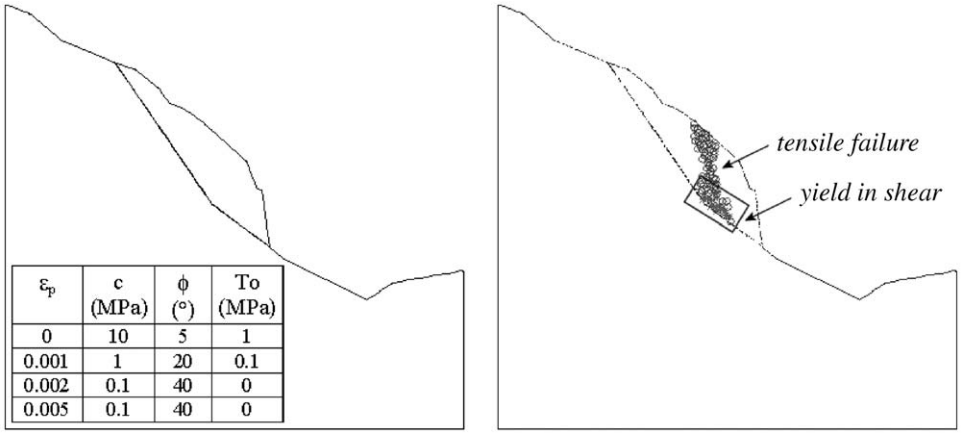

ε_p	c (MPa)	ϕ (°)	To (MPa)
0	10	5	1
0.001	1	20	0.1
0.002	0.1	40	0
0.005	0.1	40	0

Fig. 22. Distinct-element strain-softening model showing development of Prandtl-type yield zone at base of slide surface and propagation of tensile damage upwards through intact slide mass, dividing the slide mass along the contact between first and second Randa rockslide events.

slide mass as a function of plastic strains. Similar to analyses performed in the previous section, intact rock strength was degraded as damage and plastic strains accumulated. Input values were approximated from brittle fracture thresholds for intact crystalline rock [43] and are provided together with the model and modelled results in Fig. 22. Results show that a zone of yield due to shear damage develops near the base of the eventual slide surface and transforms into a tensile failure zone in the upper slide body as straining occurs. This zone of tensile damage continues through the intact slide mass dividing the rockslide into two distinct blocks, approximating the boundary between the first and second Randa slide events. This provides a first indication that the episodic nature of the slide may have been partly driven by internal brittle fracture damage that developed over time due to stress concentrations and strength degradation. The tensile mode of damage suggested by the model also supports the strain-dependent frictional strength development concept introduced by Hajiabdolmajid and Kaiser [41].

To more closely examine these mechanisms, further modelling was performed using the hybrid finite-/discrete-element approach concentrating on the Rankine tensile crack constitutive model. As before, the model was set up without the inclusion of a pre-existing failure plane allowing for modelled failure to progressively develop through internal fracturing and shearing. Fig. 23 shows that these results predict a staged failure. The first stage involves the progressive internal

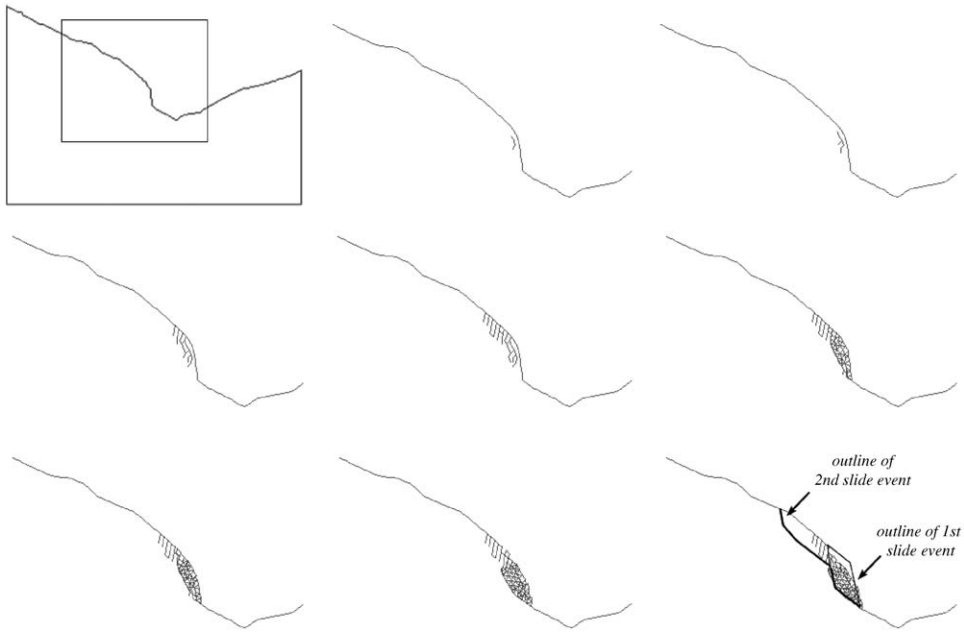

Fig. 23. Hybrid finite-/discrete-element model results focussing on internal deformation to reproduce staged nature of the 1991 Randa rockslide (using a Rankine tensile fracture constitutive model).

fracturing of the rock mass leading to collapse of the frontal region of the slope. This staged development was also seen in Fig. 20 where the Mohr–Coulomb with Rankine tension cutoff constitutive model was used. The modelled slide boundaries for this first failure stage closely approximate those of the first Randa slide event (April 18, 1991; Fig. 7), and its progressively disintegrating nature would agree well with observations that the event lasted several hours and involved the tilting and falling of large blocks one after another [44]. Such a mode of failure would require extensive internal deformation, fracturing and dilation, as demonstrated by the models. In contrast, if the slide mass would have failed as a more coherent intact mass, then catastrophic failure would likely have occurred as a sudden collapse on a time scale of minutes instead of periodically over several hours (examples of this would be the aforementioned Goldau and Elm rockslides shown in Fig. 5).

A second consequence of the internal fracturing and periodic disintegration of the slide mass during this first failure interval was that the slide debris deposited itself at the toe of the slope as opposed to evolving into a longer runout. Fig. 24 shows both the April 18 and May 9, 1991 Randa slide events plotted on Heim's Fahrböschung plot as reproduced by Schindler et al. [19]. The plot shows that given the volumes of the two slide events, their runout distances were significantly shorter than those seen for other large rockslides of comparable volumes. The model results shown in Fig. 23 concur and help to explain the shorter than normal runout achieved by the first Randa slide event by suggesting that although the potential energy of the slide mass may be equal whether it is coherent or fractured: (1) internal friction mobilized as a consequence of internal fracturing would act to reduce the kinetic energy available to drive the mass, thereby reducing the runout reach of the event; and (2) if the slide mass does not fail as a singular event but periodically over a period of several hours, then the potential energy and corresponding momentum of the mass is not a function of the entire failed volume (e.g. 20 million m^3 as reported in the case of the first Randa slide event) but that of the individual episodic events comprised of smaller volumes. Thus smaller masses with less momentum would result in smaller runout reaches, meaning that the volume plotted in Fig. 23 for the first Randa slide event and the corresponding comparison to its runout travel angle is misleading.

Following the collapse of the rock mass during the first slide event, the model results show the development of a second sliding phase (corresponding to the May 9, 1991 event) in the form of a series of large blocks bounded by sub-vertical tension cracks that form through brittle fracturing. As was seen in results for the first sliding phase, these blocks then periodically fail in accordance with the progressive development of the second-phase basal shear plane. This again would agree with observations with respect to the nature of the second slide event described as also having occurred over several hours, and for which the runout of the failed volume ($\sim$10 million m^3) fell far short of that which would be expected based on other large rockslides.

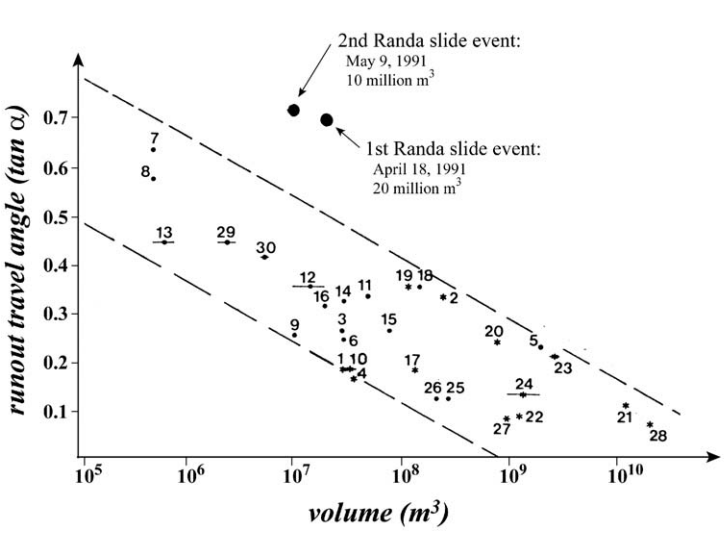

#	Location	Year
1	Sherman (Alaska)	1964
2	Vajont (Italien)	1963
3	Madison (USA)	1959
4	Gros Ventre (USA)	1925
5	Pamir	1911
6	Frank (Kanada)	1903
7	Airolo	1898
8	Schächental	1887
9	Elm	1881
10	Goldau	1806
11	Diablérets	1714/49
12	Disentis	1683
13	Val Lagone	1486
14	Voralpsee	pre-historic
15	Scima da Saoseo	"
16	Corno di Dosdé	"
17	Kandertal	"
18	Poschiavo	"
19	Obersee GL	"
20	Glärnisch-Guppen	"
21	Flims	"
22	Tamins	"
23	Engelberg	"
24	Siders	"
25	Blackhawk (USA)	"
26	Silver Reef (USA)	"
27	Fernpass (Oesterreich)	"
28	Saidmarreh (Iran)	"
29	Wengen, S Chneugraben	"
30	Wengen, Chneugraben	"

Fig. 24. Plot of Albert Heim's Fahrböschung ($\tan\alpha$) versus rock slide volume showing the runout characteristics of the two Randa slide events with respect to other large volume rockslides (after Schindler et al. [19]). The Fahrböschung (α), or travel angle, is simply measured as the angle of the line taken from the top of the slide scarp to the toe of the runout (i.e. higher travel angles reflect shorter slide runouts).

4. Discussion and conclusions

Evans [45] estimates that on a global level a massive rock slope failure (>20 million m^3) occurs every 3.2 years. Given that prior to their failure, these natural slopes had experienced apparent periods of stability lasting thousands of years over which few major external changes had occurred with respect to their kinematic state (e.g. since the loss of confinement along valley walls during glacial retreat), the temporal evolution of rock mass strength degradation through processes like progressive failure must be considered to explain their periodicity. As demonstrated in this study, the framework of the progressive failure conceptual model requires the consideration of two factors: slide plane development and internal rock mass deformation/degradation.

Various numerical techniques (i.e. continuum and discontinuum methods, and hybrid methods which combine both continuum and discontinuum methodologies to simulate brittle fracturing) have been applied here to demonstrate the evolution of failure in massive natural rock slopes as a function of slide plane development and internal strength degradation. In this case, the initiation and development of the 1991 Randa rockslide was focussed on. Results incorporating concepts related to progressive strength degradation and failure clearly show that in the instance of the 1991 Randa rockslide, pre-existing fully persistent geological structures are not necessary to explain failure. Instead, both continuum (finite-element) and hybrid (finite-/discrete-element) results show that the failure process could have initiated through the development of tensile rock mass damage following deglaciation of the valley below the slope. Redistributed stress concentrations resulting from oversteepening of the slopes would then intensify fracture propagation and coalescence within these damage zones, leading to the progressive development of a failure surface extending from two or more damage initiation centres.

When initiation processes were modelled using hybrid techniques in combination with a Mohr–Coulomb shear fracture constitutive model with tension cutoff, the failure surface was observed to form through the development of sub-vertical tensile fractures normal to the direction of downslope movement. As the density of these fractures increased, the shear plane progressively developed perpendicular to them forming a curvilinear failure surface typical of more ductile failures. When employing the Rankine tensile fracture constitutive model, the fractures were observed to form parallel to the surface topography, more closely approximating the irregular nature of the 1991 Randa failure surface. In both cases, the process was largely driven by the initial formation of brittle tensile fractures, eventually leading to shear failure and mobilization once the rock mass coherence was significantly degraded. In other words, shear only became a factor after enough tensile fracture damage was incurred to allow mobilization. The final profile of the failure surface, however, would largely be influenced by the interaction of the prevailing discontinuity network and fractures generated through either tension or shear.

Further results based on discontinuum (distinct-element) and hybrid models also show that internal deformation and damage within the slope mass due to

strength degradation would result in brittle–ductile transition processes sub-dividing the slide mass into two key blocks through sub-vertical tensile brittle fracturing. These model results closely agree with the observed boundaries delineating the two slide events constituting the 1991 Randa rockslide. The inclusion of explicit tensile brittle fracture processes through the use of hybrid modelling techniques helped to provide important insight as to the underlying mechanisms corresponding to the episodic nature of the rocklide and its relatively short runout distances when compared to other major rockslides of comparable volumes.

Today, the remaining rock slope mass above the 1991 Randa rockslide scarp still shows signs of activity with displacement rates of 1–2 cm/year (as measured since 1991). This may be interpreted as a third phase of the rockslide as the slope mass tries to reach a stable slope geometry. The current unstable mass is bounded by deep, active, sub-vertical tension cracks and has a potential volume of up to 2.5 million m^3. For this reason, Randa is the subject of an ongoing investigation relating to the in situ monitoring of a progressively developing failure in a massive rock slope using instrumentation systems designed to measure temporal and 3-D spatial relationships between fracture systems, displacements, pore pressures and microseismicity [20]. Ongoing work aims at improving the modelling of progressive failure concepts by constraining them with field measurements, while also investigating the influence of pre-existing discontinuities, fatigue, comminution and transport on the failure and runout process.

Acknowledgements

The authors wish to thank Heike Willenberg, Dr. Peter Kaiser and Prof. Simon Loew for their contributions to this work. Support and material relating to ELFEN, provided by Rockfield Software, was greatly appreciated. Funding for this project was provided in part through a grant from the Swiss National Science Foundation (Project No. 2100-059283.99).

References

[1] Terzaghi K. Stability of steep slopes on hard unweathered rock. Géotechnique 1962;12:251–70.
[2] Robertson AM. The interpretation of geological factors for use in slope theory. In: Planning Open Pit Mines, Proceedings, Johannesburg, 1970. p. 55–71.
[3] Einstein HH, Veneziano D, Baecher GB, O'Reilly KJ. The effect of discontinuity persistence on rock slope stability. Int J Rock Mech Min Sci Geomech Abstr 1983;20(5):227–36.
[4] Eberhardt E, Willenberg H, Loew S, Maurer H. Active rockslides in Switzerland—understanding mechanisms and processes. In: International Conference on Landslides—Causes, Impacts and Countermeasures, Davos, 2001. p. 25–34.
[5] Bjerrum L. Progressive failure in slopes of overconsolidated plastic clay and clay shales. J Soil Mech Foundat Div ASCE 1967; 93(SM5):1–49.
[6] Lajtai EZ. Strength of discontinuous rocks in direct shear. Géotechnique 1969;19(2):218–33.
[7] Jennings JE. A mathematical theory for the calculation of the stability of slopes in open cast mines. In: Planning Open Pit Mines, Proceedings, Johannesburg, 1970. p. 87–102.
[8] Jaeger JC. Friction of rocks and stability of rock slopes—11th Rankine Lecture. Géotechnique 1971;21(2):97–134.
[9] Barton N. Progressive failure of excavated rock slopes. In: Stability of Rock Slopes, Proceedings of the 13th US Symposium on Rock Mechanics, Urbana, IL, 1971. p. 139–70.
[10] Einstein HH, Lee JS. Topological slope stability analysis using a stochastic fracture geometry model. In: Proceedings of the Conference on Fractured and Jointed Rock Masses, Lake Tahoe, 1995. p. 89–98.
[11] Scavia C. A method for the study of crack propagation in rock structures. Géotechnique 1995;45(3):447–63.
[12] Kaneko K, Otani J, Noguchi Y, Togashiki N. Rock fracture mechanics analysis of slope failure. In: Deformation and Progressive Failure in Geomechanics, Nagoya, Japan, 1997. p. 671–76.
[13] Heim A. Bergsturz und menschenleben. Zurich: Fretz and Wasmuth Verlag; 1932.
[14] Mencl V. Mechanics of landslides with non-circular slip surfaces with special reference to the Vaiont slide. Géotechnique 1966;16(4):329–37.
[15] Sarma SK. Stability analysis of embankments and slopes. J Geotech Eng Div ASCE 1979;105(GT12):1511–34.
[16] Martin CD, Kaiser PK. Analysis of rock slope with internal dilation. Can Geotech J 1984;21(4):605–20.
[17] Götz A, Zimmermann M. The 1991 rock slides in Randa: causes and consequences. Landslide News 1993;7:22–5.
[18] Noverraz F, Bonnard C. L'écroulement rocheux de Randa, prés de Zermatt. In: Proceedings of the Sixth International Symposium on Landslides, Christchurch, 1991. p. 165–70.
[19] Schindler C, Cuénod Y, Eisenlohr T, Joris C-L. Die Ereignisse vom 18. April und 9. Mai 1991 bei Randa (VS)—ein atypischer Bergsturz in Raten. Eclogae Geol Helv 1993;86(3):643–65.
[20] Willenberg H, Spillmann T, Eberhardt E, Evans K, Loew S, Maurer H. Multidisciplinary monitoring of progressive failure processes in brittle rock slopes—concepts and system design. In: Proceedings of the first European Conference on Landslides, Prague, 2002. p. 477–83.
[21] Evans SG, Clague JJ, Woodsworth GJ, Hungr O. The Pandemonium Creek rock avalanche, British Columbia. Can Geotech J 1989;26:427–46.
[22] Stead D, Eberhardt E, Coggan J, Benko B. Advanced numerical techniques in rock slope stability analysis—applications and limitations. In: International Conference on Landslides—Causes, Impacts and Countermeasures, Davos 2001. p. 615–24.
[23] VIPS.VISAGE—vectorial implementation of structural analysis, geotechnical engineering, Version 8.0. Winkfield-Windsor: Vector International Processing Systems Ltd; 2001.
[24] Itasca. FLAC—fast Lagrangian analysis of continua, version 4.0. Minneapolis: Itasca Consulting Group, Inc.; 2000.
[25] Stead D, Eberhardt E. Developments in the analysis of footwall slopes in surface coal mining. Eng Geol 1997;46(1):41–61.
[26] Itasca. UDEC—universal distinct element code, version 3.1. Minneapolis: Itasca Consulting Group, Inc.; 2000.
[27] Munjiza A, Owen DRJ, Bicanic N. A combined finite-discrete element method in transient dynamics of fracturing solids. Eng Comput 1995;12:145–74.
[28] Rockfield. ELFEN 2D/3D numerical modelling package, version 3.0. Swansea: Rockfield Software Ltd.; 2001.

[29] Yu J. A contact interaction framework for numerical simulation of multi-body problems, aspects of damage and fracture for brittle materials. PhD thesis, University of Wales, 1999.
[30] Klerck PA. The finite element modelling of discrete fracture of quasi-brittle materials. PhD thesis, University of Wales, 2000.
[31] Crook T, Willson S, Yu JG, Owen R. Computational modelling of the localized deformations associated with borehole breakout in quasi-brittle materials. J Pet Sci Eng 2003;31(3–4):177–86.
[32] Stead D, Eberhardt E, Benko B. The influence of horizontal stresses on the stability of surface coal mine footwall slopes. In: Proceedings of the Fourth International Symposium on Mine Planning and Equipment Selection, Calgary, 1995. p. 1075–80.
[33] Chowdhury RN. Understanding landslides in relation to initial ground stresses. In: Proceedings of the Second International Symposium on Landslides and their Control, Tokyo, 1977. p. 33–9.
[34] Kastrup U, Zoback ML, Deichmann N, Evans K, Michael AJ, Giardini D. Stress field variations in the Swiss Alps and the northern Alpine foreland derived from inversion of fault plane solutions. J Geophys Res 2003, in press.
[35] Hoek E, Bieniawski ZT. Brittle fracture propagation in rock under compression. Int J Fract Mech 1965;1(3):137–55.
[36] Huang J, Wang Z, Zhao Y. The development of rock fracture from microfracturing to main fracture formation. Int J Rock Mech Min Sci Geomech Abstr 1993;30(7):925–8.
[37] Eberhardt E, Stead D, Stimpson B, Read RS. Identifying crack initiation and propagation thresholds in brittle rock. Can Geotech J 1998;35(2):222–33.
[38] Glasser NF. The origin and significance of sheet joints in the Cairngorm granite. Scott J Geol 1997;33(2):125–31.
[39] Florineth D, Schlüchter C. Reconstructing the Last Glacial Maximum (LGM) ice surface geometry and flowlines in the Central Swiss Alps. Eclogae Geol Helv 1998;91(3):391–407.
[40] Schulson EM. The structure and mechanical behaviour of ice. JOM: Minerals Metals Mater Soc 1999;51(2):21–7.
[41] Hajiabdolmajid V, Kaiser PK. Slope stability assessment in strain-sensitive rocks. In: EUROCK 2002, Proceedings of the ISRM International Symposium on Rock Engineering for Mountainous Regions, Funchal, Madeira, 2002. p. 237–44.
[42] Eberhardt E, Stead D, Coggan J, Willenberg H. An integrated numerical analysis approach to the Randa rockslide. In: Proceedings of the First European Conference on Landslides, Prague, 2002. p. 355–62.
[43] Eberhardt E, Stead D, Stimpson B. Quantifying pre-peak progressive fracture damage in rock during uniaxial loading. Int J Rock Mech Min Sci 1999;36(3):361–80.
[44] Bonnard C, Noverraz F, Lateltin O, Raetzo H. Large landslides and possibilities of sudden reactivation. Felsbau 1995;13(6):401–7.
[45] Evans SG. Single-event landslides resulting from massive rock slope failure: characterising their frequency and impact on society. NATO Advanced Research Workshop on Massive Rock Slope Failure: New Models for Hazard Assessment, NATO Science Series IV: Earth and Environmental Sciences, 2003, in press.